Environmental Science & Technology

pubs.acs.org/est

Article

Deposition and Re-Emission of Atmospheric Elemental Mercury over the Tropical Forest Floor

Wei Yuan, Xun Wang,* Che-Jen Lin, Qinghai Song, Hui Zhang, Fei Wu, Nantao Liu, Huazheng Lu, and Xinbin Feng*

Cite This: *Environ. Sci. Technol.* 2023, 57, 10686−10695

Read Online

ACCESS | Metrics & More | Article Recommendations | Supporting Information

ABSTRACT: Significant knowledge gaps exist regarding the emission of elemental mercury (Hg^0) from the tropical forest floor, which limit our understanding of the Hg mass budget in forest ecosystems. In this study, biogeochemical processes of Hg^0 deposition to and evasion from soil in a Chinese tropical rainforest were investigated using Hg stable isotopic techniques. Our results showed a mean air−soil flux as deposition of −4.5 ± 2.1 ng m^{-2} h^{-1} in the dry season and as emission of +7.4 ± 1.2 ng m^{-2} h^{-1} in the rainy season. Hg re-emission, i.e., soil legacy Hg evasion, induces negative transitions of Δ^{199}Hg and δ^{202}Hg in the evaded Hg^0 vapor, while direct atmospheric Hg^0 deposition does not exhibit isotopic fractionation. Using an isotopic mass balance model, direct atmospheric Hg^0 deposition to soil was estimated to be 48.6 ± 13.0 μg m^{-2} $year^{-1}$. Soil Hg^0 re-emission was estimated to be 69.5 ± 10.6 μg m^{-2} $year^{-1}$, of which 63.0 ± 9.3 μg m^{-2} $year^{-1}$ is from surface soil evasion and 6.5 ± 5.0 μg m^{-2} $year^{-1}$ from soil pore gas diffusion. Combined with litterfall Hg deposition (~34 μg m^{-2} $year^{-1}$), we estimated a ~12.6 μg m^{-2} $year^{-1}$ net Hg^0 sink in the tropical forest. The fast nutrient cycles in the tropical rainforests lead to a strong Hg^0 re-emission and therefore a relatively weaker atmospheric Hg^0 sink.

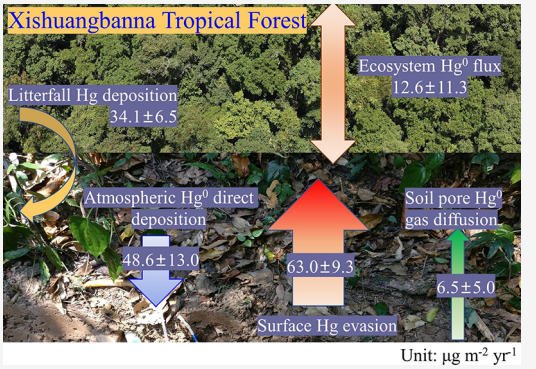

KEYWORDS: *mercury isotope, tropical forest, air−soil mercury exchange, mass balance model, legacy mercury re-emission*

1. INTRODUCTION

Mercury (Hg) is a persistent pollutant that causes health and ecological concerns across the globe due to the long-range transport of its gaseous elemental form (GEM, Hg^0) via atmospheric circulation.[1,2] Globally, forest ecosystems represent a significant atmospheric sink (with 2100−3200 Mg $year^{-1}$) of total atmospheric Hg^0, equivalent to 40−65% of the total Hg pool in the atmosphere (5000−5600 Mg).[3,4] Quantification of Hg deposition and re-emission in forest ecosystems is the foundation to understand the global Hg mass budget. Earlier studies have documented Hg biogeochemical cycles in temperate and boreal forest ecosystems.[5−8] However, the data remain scarce for tropical forests, which account for 45% of the global forest areas.[9] It had been postulated that tropical forests have the largest soil Hg storage and litterfall Hg sink among the terrestrial ecosystems across the globe.[10,11] These initial findings required further investigation to better understand the global Hg budget in forest ecosystems.

Tropical forests have unique climate, vegetation, and biogeochemical cycles. The warm and wet climatic conditions produce a large amount of biomass and a canopy height over 25 m.[12] Litter decomposition is comparatively rapid with >95% mass loss within a year,[13] leading to highly productive tropical forests often with nutrient-poor soils.[14] One important question is that the high biodiversity and nutrient turnover in tropical rainforests[15,16] likely result in the tropical Hg accumulation and sequestration different from other forest types.[17] Litterfall Hg deposition in tropical rainforests was estimated to be 34−75 μg m^{-2} $year^{-1}$, 1−2 times higher than that in subtropical forests and 2−5 times higher than that in temperate and boreal forests (10−20 μg m^{-2} $year^{-1}$).[10,17−19] The reported elevated litterfall Hg deposition does not seem to lead to a correspondingly higher Hg concentration of surface soil compared to other forests.[17,18,20−25] This raises questions that the warm and wet conditions in tropical rainforests potentially cause elevated Hg^0 re-emissions from the forest floor. Measurements of air−soil Hg^0 exchange in tropical rainforests remain few, existing data points to the forest soil being a net atmospheric Hg^0 source with uncertainties because of limited data availability and soil spatial heterogeneities.[26−28]

Received: February 13, 2023
Revised: June 8, 2023
Accepted: June 29, 2023
Published: July 12, 2023

Air−soil Hg^0 flux over the forest floor is a result of complicated bidirectional processes, including Hg^0 evasion from forest soil and direct atmospheric Hg^0 deposition.[29−32] Existing measurement of air−soil Hg^0 flux using a flux chamber only represents a net flux and does not provide insight regarding the source and sink terms. The microbial and organic degradation in soil and the photoreduction at the air−soil interface facilitate Hg^0 evasion from the forest floor[5,33] at various degrees depending on forest types and environmental conditions. Fractionation of stable Hg isotopes, quantified as mass-dependent fractionation (MDF, reported as δ^{202}Hg), odd mass-independent fractionation (odd-MIF, reported as Δ^{199}Hg and Δ^{201}Hg), and even mass-independent fractionation (even-MIF, reported as Δ^{200}Hg and Δ^{204}Hg), is an effective tracing signal for Hg biogeochemical processes during air−soil Hg^0 exchange.[34] Earlier studies have documented that microbial reduction does not induce the odd-MIF shift.[35,36] Organic matter-induced dark reduction is associated with a small positive odd-MIF in the product Hg^0 (<0.3‰).[37] Photoreduction leads to a relatively large positive odd-MIF in the product Hg^0 of Hg and organic sulfur complexes.[38−40] The Hg odd-MIF signals can be utilized to quantify the contribution from the individual Hg biogeochemical process to soil Hg emission flux.

We hypothesized that the high nutrient turnover in tropical rainforests effectively facilitates Hg^0 re-emission from the forest floor. The objective of this study is to quantify the contribution of individual Hg biogeochemical processes underlying the air−soil Hg^0 exchange in a Chinese tropical rainforest using isotopic tracing techniques. We measured the vertical distribution of Hg^0 concentrations and isotopic fingerprints in ambient air and the gas samples from the inlet and outlet of a dynamic flux chamber using ambient and Hg-free air. We discussed the implications of Hg re-emission from tropical forests in relation to the global forest Hg mass budget.

2. MATERIALS AND METHODS

2.1. Site Description. The study site locates at 725−766 m above the sea level (asl) within the P55 Tropical Forest Dynamic Plot (P55, 21°57′40″N, 101°12′1.08″E) in Xishuangbanna, Yunnan Province in Southwest China. The P55 plot was located at the northern edge of the tropical region,[9] showing a tropical monsoon climate with an annual mean temperature of 22.6 °C and precipitation of 1350 mm.[17] The year-round frost-free condition is a representative feature of tropical climate. There is a distinct dry season (November−April) and a rainy (May−October) season. The precipitation in the rainy season accounts for ∼87% of total annual precipitation. The dominant tree species of the plot are *Pometia pinnata* and *Barringtonia fusicarpa* with a canopy height of 30−45 m.[17,41] The vegetation represents a typical tropical rainforest.[42,43] The mineral soil is composed of limestone-derived soils with pH values of 4.5−5.5.[42]

2.2. Field Observations and Sample Collections. We measured the vertical profile of Hg^0 concentrations at 2 m above the forest floor, 5 cm above the forest floor, and soil pore Hg^0 gas at 10, 20, and 40 cm depth of soil. We also conducted measurements of air−soil Hg^0 exchange flux in August 2019 (representing the rainy season) and from December 2020 to January 2021 (representing the dry season) (Section S1). Simultaneously, the environmental parameters including air and soil temperature, soil moisture (by volume content of soil), and photosynthetically active radiation (PAR) were measured nearby the measurement plot.

The abovementioned protocols have been described in detail in our previous work.[34,44] Briefly, a Teflon tube with a 1/4 inch outer diameter covered a 0.22 μm pore size, and a 13 mm-diameter polytetrafluoroethylene filter was utilized for collecting soil pore gas. The Hg^0 concentration was measured using an automated Hg vapor analyzer (Model 2537X, Tekran Instruments Corp., Canada) via a synchronized eight-port sampling system (Tekran Model 1115). The time resolution was 5 min for Hg^0 during the rainy season and 15 min during the dry season due to the lower soil gas content. Three replicate air−soil Hg^0 exchange flux measurements were made. Each flux measurement cycle ranged from 4 to 6 days during the rainy season and from 8 to 10 days during the dry season by using a novel dynamic flux chamber (NDFC), as described in our earlier work.[44,45] The air−soil Hg^0 flux was calculated as follows:

$$F_{Hg^0} = \frac{Q \times (C_{outlet} - C_{inlet})}{S_{NDFC}} \quad (1)$$

where F_{Hg^0} is the Hg^0 flux (ng m^{-2} h^{-1}); Q is the internal flushing flow rate (m^3 h^{-1}, nearly 0.6 in this study); S_{NDFC} is the NDFC footprint area (m^2, 0.09 m^2 in this study); and C_{inlet} and C_{outlet} represent the Hg^0 concentration at the NDFC inlet and outlet, respectively. A positive F_{Hg^0} means Hg^0 emission from the forest soil to the atmosphere, while a negative F_{Hg^0} means atmospheric Hg^0 deposition onto the forest soil. Exposure by Hg-free air was used for eliminating Hg^0 deposition into the soil and therefore only measuring the unidirectional potential Hg^0 evasion rate from soil. Stable Hg isotope sampling in soil pore gas and during air−soil Hg^0 exchange has been described in our earlier work.[34] Briefly, we used 0.8 g of chlorine-impregnated activated carbon (ClC) traps[46] with a flow rate of 8−10 L min^{-1} to collect the air gas from 2 m above the forest floor, 5 cm above the forest floor, and the outlet of the flux chamber. The ClC trap collects total gaseous mercury (TGM). Since the GEM concentration accounts for more than ∼98% of TGM in a remote forest of Southwestern China,[47,48] the isotopic signatures of Hg collected by the ClC trap realistically represent GEM isotopic compositions in this study.

2.3. Measurements of Hg Isotopes. The pre-concentration of ClC-trap samples and measurements of isotopic compositions were made at the State Key Laboratory of Environmental Geochemistry, Institute of Geochemistry, Chinese Academy of Sciences, followed by our previous studies.[21,34,49,50] Briefly, the ClC traps were processed by the double-stage heating pyrolysis in a tube muffle furnace[51] using 25 mL min^{-1} of high-purity oxygen with 5 mL of oxidizing trapping solution of 40% mixture of concentrated nitric and hydrochloric acid ("reverse aqua regia", HNO_3/HCl = 2:1, v/v). The trapping solution Hg concentration was analyzed by cold vapor atomic fluorescence spectrometry using the US-EPA method 1631.[52] Then, the diluted Hg^{II} trapping solution with 1 ng mL^{-1} was measured for Hg isotope compositions using a multi-collector inductively coupled plasma mass spectrometer (MC-ICPMS, Neptune II, Thermo Scientific, USA). Following the calculation of Bergquist and Blum,[53] MDF is reported as

https://doi.org/10.1021/acs.est.3c01222
Environ. Sci. Technol. 2023, 57, 10686−10695

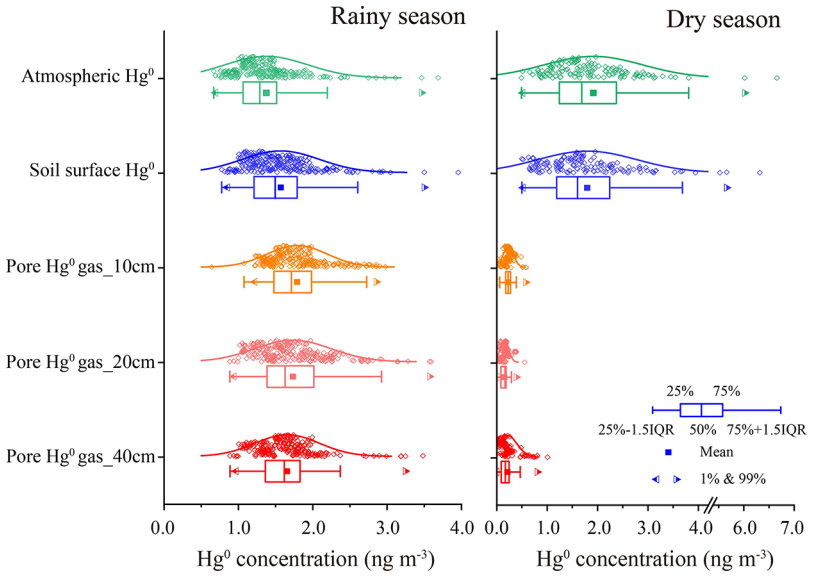

Figure 1. Box charts for atmospheric Hg^0 concentration at 2 m above ground, in near-surface air, 10 cm soil pore gas, 20 cm soil pore gas, and 40 cm soil pore gas in rainy and dry seasons, respectively.

$$\delta^{202}\mathrm{Hg}\ (‰) = [(^{202}\mathrm{Hg}/^{198}\mathrm{Hg})_{\mathrm{sample}}/(^{202}\mathrm{Hg}/^{198}\mathrm{Hg})_{\mathrm{ref}} - 1] \times 1000 \quad (2)$$

MIF is calculated as

$$\Delta^{xx}_{x}\mathrm{Hg}\ (‰) = \delta^{xx}_{x}\mathrm{Hg} - \delta^{202}\mathrm{Hg} \times \beta_{xxx} \quad (3)$$

where β_{xxx} is 0.252 for ^{199}Hg, 0.502 for ^{200}Hg, and 0.752 for ^{201}Hg, respectively. $(^{202}\mathrm{Hg}/^{198}\mathrm{Hg})_{\mathrm{ref}}$ represents the result in a standard sample, NIST 3133. The NIST 3177 (UM-Almadén standard solution), as a secondary standard, was measured every 10 samples during the isotope measurement, which was determined as δ^{202}Hg = −0.49 ± 0.10, Δ^{199}Hg = 0.00 ± 0.06, Δ^{200}Hg = 0.01 ± 0.08, and Δ^{201}Hg = 0.01 ± 0.10‰ (mean ± 2σ, n = 6). The certified reference material of BCR-482 (Lichen) and GSS-4 (calcific soil) was combusted in an oven-enrichment system at a frequency of every 10 samples to test the potential isotopic bias. The measured isotope signatures of BCR-482 were δ^{202}Hg = −1.49 ± 0.03, Δ^{199}Hg = −0.62 ± 0.09, Δ^{200}Hg = 0.05 ± 0.08, and Δ^{201}Hg = −0.58 ± 0.12‰ (±2σ, n = 3) and of GSS-4 as δ^{202}Hg = −1.60 ± 0.05, Δ^{199}Hg = −0.46 ± 0.03, Δ^{200}Hg = 0.00 ± 0.06, and Δ^{201}Hg = −0.42 ± 0.06‰ (±2σ, n = 6), consistent with the reported values,[50,54] suggesting few biases induced during pre-concentration by a double-stage offline combustion-trapping technique.

2.4. Hg Isotopic Mass Balance Model. We used a mass balance model of Hg isotopes to quantify the contribution of Hg^0 deposition and evasion that occurred at the surface of topsoil and soil pore Hg^0 emission. The modeling configuration has been described in detail in our earlier study:[34]

$$M_{\mathrm{inlet}} + M_{\mathrm{top}} + M_{\mathrm{emi}} = M_{\mathrm{outlet}} + M_{\mathrm{dep}} \quad (4)$$

$$M_{\mathrm{inlet}}\cdot\Delta^{199}\mathrm{Hg}_{\mathrm{atm}} + M_{\mathrm{top}}\cdot\Delta^{199}\mathrm{Hg}_{\mathrm{top}} + M_{\mathrm{emi}}\cdot\Delta^{199}\mathrm{Hg}_{\mathrm{emi}} = M_{\mathrm{outlet}}\cdot\Delta^{199}\mathrm{Hg}_{\mathrm{exc}} + M_{\mathrm{dep}}\cdot\Delta^{199}\mathrm{Hg}_{\mathrm{atm}} \quad (5)$$

$$M_{\mathrm{top}}\cdot\Delta^{199}\mathrm{Hg}_{\mathrm{top}} + \xi\cdot M_{\mathrm{emi}}\cdot\Delta^{199}\mathrm{Hg}_{\mathrm{emi}} = (M_{\mathrm{top}} + \xi\cdot M_{\mathrm{emi}})\cdot\Delta^{199}\mathrm{Hg}_{\mathrm{zero-exc}} \quad (6)$$

where M_{inlet}, M_{outlet}, M_{dep}, M_{top}, and M_{emi} represent the Hg^0 flux of the inlet of the chamber, outlet of the chamber, atmospheric deposition into the chamber, topsoil evasion in the chamber, and soil pore gas diffusion in the chamber, respectively (ng m^{-2} h^{-1}). $\Delta^{199}\mathrm{Hg}_{\mathrm{atm}}$, $\Delta^{199}\mathrm{Hg}_{\mathrm{top}}$, $\Delta^{199}\mathrm{Hg}_{\mathrm{emi}}$, $\Delta^{199}\mathrm{Hg}_{\mathrm{exc}}$, and $\Delta^{199}\mathrm{Hg}_{\mathrm{zero-exc}}$ represent the $Hg^0\Delta^{199}$Hg signature of near-surface ambient air, Hg^0 reduction that occurred at topsoil, soil pore gas, and efflux under ambient air and Hg-free air, respectively. ξ is a correction factor to offset the increased emission-driven change in the data collected with Hg-free air and can be estimated by

$$\xi = \frac{C^{\mathrm{Hg}^0}_{\mathrm{soil-pore}}}{C^{\mathrm{Hg}^0}_{\mathrm{soil-pore}} - C^{\mathrm{Hg}^0}_{\mathrm{surface}}} \quad (7)$$

where $C^{\mathrm{Hg}^0}_{\mathrm{soil-pore}}$ represents the Hg^0 concentration in 10 cm soil pore gas, and $C^{\mathrm{Hg}^0}_{\mathrm{surface}}$ represents the Hg^0 concentration in near-surface air.

2.5. Quality Assurance/Quality Control and Statistical Methods. To eliminate cross-contamination during field observation, the tubing inlet, Teflon filter, and soda-lime scrubber in the inlet of the Tekran 2537X were changed in each experiment period. The Tekran 2537X was calibrated before each flux measurement to ensure the difference between two gold tubes within 3% and the peak area within 5%. The field blank of ClC traps was determined to be 150−300 pg g^{-1}, less than 3% of the amount loaded after an experiment. The breakthrough of ClC traps is lower than 0.6% under a gas rate of 10 L min^{-1}. The ability of the ClC to capture gaseous Hg^0 ranges between 90 and 108% (n = 31), which does not induce Hg isotopic fractionation.[46,55]

We used the conceptual structural equation model (SEM) to quantify interplays among environmental parameters (air temperature, soil water content, and PAR), gas Hg^0 concentration (air and soil pore gas), and air−soil exchange flux. SEM was developed by using χ^2 tests with maximum likelihood estimations. More detailed information has been described in our earlier studies.[11,44] Briefly, all variables were standardized into Z scores using SPSS version 17, and model

https://doi.org/10.1021/acs.est.3c01222
Environ. Sci. Technol. 2023, 57, 10686−10695

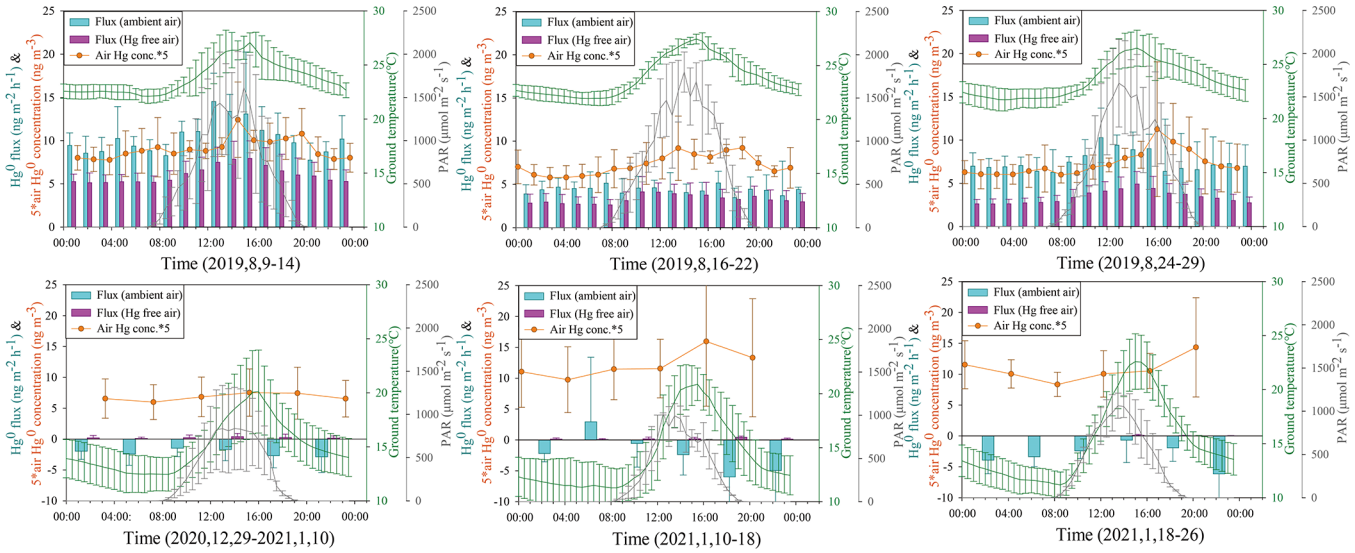

Figure 2. Diurnal variation of air−soil Hg^0 flux and environmental parameters. The error bar is ±1 standard deviation of multiple day observations. The column filled with cyan and purple represents the air−soil Hg^0 flux under ambient air exposure and Hg-free gas exposure, respectively. The green line represents the 5 cm above ground temperature (°C). The orange line represents the 5 times air Hg^0 concentration (ng m^{-3}). The error bars represent ±1 standard deviation.

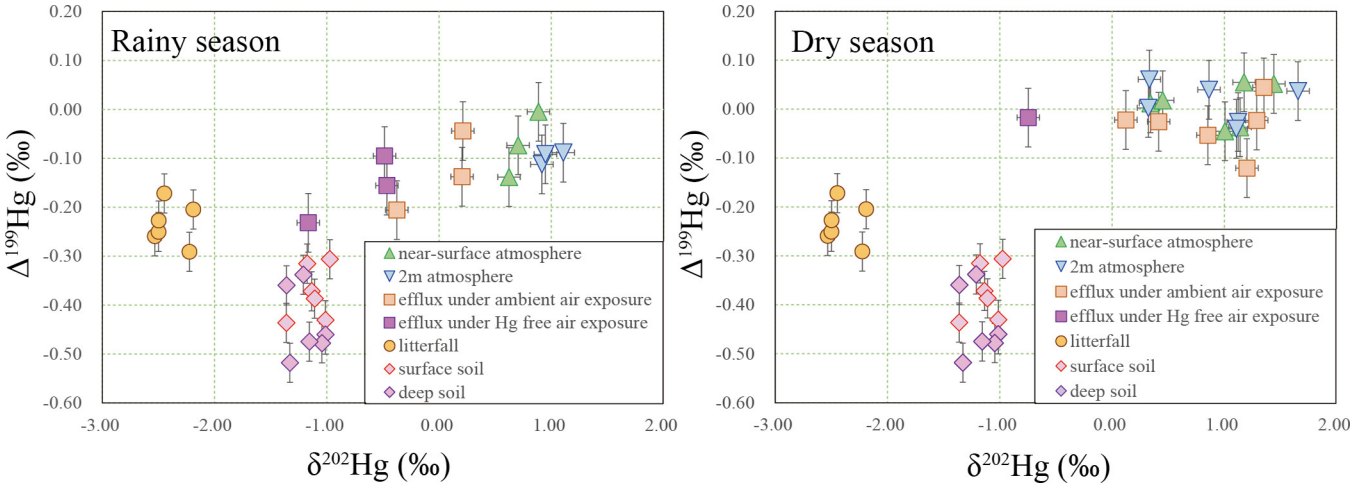

Figure 3. Observed Hg isotopic compositions (Δ^{199}Hg vs δ^{202}Hg) in each compartment of the tropical forest ecosystem. The litterfall (orange filled circles), surface soil (pink filled diamonds), and deep soil (purple filled diamonds) isotopic data were from Xia et al.[17] The error bars represent ±2 standard deviation.

fitting was performed by Amos software version 24. From the SEM path network, the standardized path coefficient (β) represents the direct effect of one variable on our targeted value. Additionally, we used independent-samples *t*-test and one-way ANOVA for significant difference analysis at a 95% confidence level when data were normally distributed. Otherwise, the Kruskal−Wallis test was applied.

3. RESULTS

3.1. Vertical Distribution of Hg^0 Concentrations. The mean and median Hg^0 concentrations in air 2 m above the forest floor were 1.38 ± 0.56 and 1.29 ng m^{-3} (N = 266) for the rainy season and 1.92 ± 0.98 and 1.68 ng m^{-3} (N = 144) for the dry season (Figure 1). The daytime atmospheric Hg^0 concentration in the rainy season was significantly higher than that in nighttime (1.47 ± 0.65 versus 1.28 ± 0.42 ng m^{-3}; p < 0.01, independent-samples *t*-test). The difference between the daytime and nighttime Hg^0 concentration is insignificant in the dry season (1.94 ± 1.00 ng m^{-3} for night versus 1.89 ± 0.96 ng m^{-3} for day).

The Hg^0 concentration in soil near-surface air was 1.57 ± 0.52 ng m^{-3} for the rainy season and 1.80 ± 0.98 ng m^{-3} for the dry season (Figure 1). The Hg^0 concentrations in soil pore gas during the rainy season showed a slight decreasing trend with soil depth from 1.79 ± 0.40 ng m^{-3} at 10 cm, 1.73 ± 0.51 ng m^{-3} at 20 cm, to 1.66 ± 0.43 ng m^{-3} at 40 cm depth of soil. The Hg^0 concentration gradient in soil pores in the dry season was much smaller than that in the rainy season, from 0.23 ± 0.10 ng m^{-3} at 10 cm, 0.15 ± 0.09 ng m^{-3} at 20 cm, to 0.21 ± 0.19 ng m^{-3} at 40 cm depth of soil (Figure S1).

3.2. Variations of Air−Soil Hg^0 Exchange Flux. Figure 2 and Table S1 show the seasonal pattern of air−soil Hg^0 exchange flux in the rainy and dry seasons. In the rainy season, the Hg^0 flux in three replicate experiments was 10.26 ± 2.19, 4.35 ± 1.38, and 7.48 ± 2.29 ng m^{-2} h^{-1}, respectively, with a mean value of 7.36 ± 1.15 ng m^{-2} h^{-1}. We observed a

https://doi.org/10.1021/acs.est.3c01222
Environ. Sci. Technol. 2023, 57, 10686−10695

clear diurnal trend for air−soil Hg^0 flux and air Hg^0 concentration with the lowest values observed at midnight and the highest values during 12:00−16:00 (Figure 2). In contrast, the Hg^0 flux in three replicate experiments in the dry season was −2.18 ± 1.81, −2.19 ± 5.26, and −3.07 ± 2.83 ng m^{-2} h^{-1} with a mean value of −2.48 ± 2.08 ng m^{-2} h^{-1} without any distinct diurnal variation. The evasion Hg^0 flux under Hg-free air exposure was 3.28−6.05 ng m^{-2} h^{-1} in the rainy season but nearly zero in the dry season (0.03−0.22 ng m^{-2} h^{-1}).

3.3. Variation of Hg Isotopic Signatures. The measured isotopic signatures in air samples at 2 m above ground were: $\delta^{202}Hg$ = 0.99 ± 0.10‰, $\Delta^{199}Hg$ = −0.10 ± 0.03‰, $\Delta^{200}Hg$ = −0.05 ± 0.05‰, and $\Delta^{201}Hg$ = −0.11 ± 0.05‰ in the rainy season and $\delta^{202}Hg$ = 0.90 ± 0.51‰, $\Delta^{199}Hg$ = 0.01 ± 0.04‰, $\Delta^{200}Hg$ = −0.01 ± 0.05‰, and $\Delta^{201}Hg$ = 0.00 ± 0.05‰ in the dry season (Figure 3). The Hg isotopic signatures in air samples near the surface were $\delta^{202}Hg$ = 0.74 ± 0.13‰, $\Delta^{199}Hg$ = −0.07 ± 0.07‰, $\Delta^{200}Hg$ = −0.02 ± 0.05‰, and $\Delta^{201}Hg$ = −0.06 ± 0.05‰ in the rainy season and slightly more positive in the dry season ($\delta^{202}Hg$ = 0.93 ± 0.44‰, $\Delta^{199}Hg$ = 0.01 ± 0.04‰, $\Delta^{200}Hg$ = 0.00 ± 0.05‰, and $\Delta^{201}Hg$ = 0.00 ± 0.05‰). In the rainy season, the Hg^0 in the exit gas of the flux chamber showed 0.01 ± 0.34‰ of $\delta^{202}Hg$, −0.13 ± 0.08‰ of $\Delta^{199}Hg$, −0.02 ± 0.03‰ of $\Delta^{200}Hg$, and −0.12 ± 0.12‰ of $\Delta^{201}Hg$, with more negative signatures under Hg-free gas exposure ($\delta^{202}Hg$ = −0.71 ± 0.40‰, $\Delta^{199}Hg$ = −0.16 ± 0.07‰, $\Delta^{200}Hg$ = −0.03 ± 0.05‰, and $\Delta^{201}Hg$ = −0.11 ± 0.11‰). In the dry season, the Hg isotopic signatures in the air samples of the chamber outlet ($\delta^{202}Hg$ = 0.87 ± 0.51‰, $\Delta^{199}Hg$ = −0.03 ± 0.05‰, $\Delta^{200}Hg$ = 0.00 ± 0.05‰, and $\Delta^{201}Hg$ = −0.03 ± 0.05‰) and inlet (i.e., near-surface air) were comparable (p > 0.05 by independent-samples t-test). The Hg^0 flux under Hg-free exposure is comparatively lower in the dry season, with Hg isotopic signatures of $\delta^{202}Hg$ = −0.75 ± 0.08‰, $\Delta^{199}Hg$ = −0.02 ± 0.03‰, $\Delta^{200}Hg$ = 0.06 ± 0.05‰, and $\Delta^{199}Hg$ = −0.06 ± 0.05‰ (Tables S2 and S3).

4. DISCUSSION

4.1. Understanding the Hg^0 Vertical Profiles. The Hg^0 concentration during the rainy season showed an increasing trend from 40 to 10 cm depth soil pore gas and a decreasing trend from the forest floor to 2 m air above ground. These trends indicate Hg^0 emission from the forest floor. The high PAR and temperature in the surface soil promote soil Hg^0 evasion by enhancing Hg^{II} photoreduction, microbial reduction, abiotic dark reduction, and gas diffusion.[36−38,56] These Hg^0 re-emission processes preferentially release lighter Hg isotopes from soil,[6,34] thus the more negative $\delta^{202}Hg$ signature in near-surface air than in air of 2 m above ground (p < 0.05, by independent-samples t-test). This is also consistent with the anticorrelation of the observed $\delta^{202}Hg$ signature between the near-surface air and net flux (Figure S2).

During the dry season, Hg^0 concentrations in soil pore gas showed comparable results at various depths, which were 8−10 times lower than in ambient air. This indicates atmospheric Hg^0 deposition (−2.48 ± 2.08 ng m^{-2} h^{-1}). The Hg MDF and odd-MIF signatures in near-surface air and 2 m air above ground are comparable, suggesting that the direct deposition did not cause an observable isotopic shift because of the relatively fast vertical transport. Compared to the rainy season, the limited rate of microbial Hg reduction in the dry season[13,57,58] largely constrains the soil pore Hg^0 gas concentrations regardless of the higher porosity of soil during this period.[44,57,58]

We compared the vertical distribution of soil pore Hg^0 concentrations to the reported values in other forest sites (Figure S3). The soil pore Hg^0 concentration varies significantly. The soil pore Hg^0 gas concentration in this tropical rainforest is lower than those found at other forest sites. Soil pore Hg^0 concentrations of 10−30 ng m^{-3} had been reported at subtropical sites (Figure S3), which were attributed to the elevated soil Hg concentrations and organic matter on the forest floor that promote Hg^{II} reduction and Hg^0 formation in soil.[57−60] Interestingly, the observed soil pore Hg^0 concentrations in the summer season were significantly higher than those found in the winter season in tropical, subtropical, and temperate forests. This is a strong indication that stronger Hg^{II} reduction occurs in summertime forests across the globe. This is also consistent with flux data that Hg^0 evasion prevails in summer.[44,61,62] Furthermore, these observations show elevated soil pore Hg^0 concentrations at 10 cm depth of soil (Figure S3), indicating that Hg reduction mainly occurs in litter-covered profiles.

4.2. Source Contribution and Mass Balance of Hg^0 Flux. Hg^0 evasion from the forest floor has been attributed to the Hg^0 re-emission from the litter decompositions associated with fast carbon cycling and photoreduction driving Hg^0 away from organic surface soil.[21,31] Pore gas Hg^0 is mainly derived from the slow deposition of organic matter (i.e., slow carbon cycling pool) in soil, followed by microbial reduction.[21] In forest soil enriched with organic matter, dark reduction also contributes to a small amount of Hg^0 production in soil pore gas.[34] These biogeochemical processes are sensitive to the change of environmental and climatic conditions. We analyzed the effect of environmental factors on air−soil Hg^0 exchange flux by SEM. In the rainy season, the effect appears to be site-specific (Figure S4). PAR, soil water content, and soil temperature are most predominant at various sites. This suggests that process heterogeneities exist on the forest floor of the same site, e.g., solar exposure inducing strong Hg photoreduction at one location while enrichment of forest floor water promoting microbial Hg reduction at another. The effect of environmental factors is weaker in the dry season because of the stronger Hg^0 deposition flux compared to the evasion from soil. Atmospheric Hg^0 concentration limits Hg^0 evasion (Figure S4) due to the concentration gradient favoring atmospheric Hg^0 deposition. The slightly varied atmospheric Hg^0 concentration resulted in no diel pattern in air−soil Hg^0 flux during the dry season.

We applied the Hg isotopic mass balance model to quantify the source contribution of air−soil Hg^0 flux using eqs 4−7. Given the negligible soil pore Hg^0 gas diffusion in the dry season, we used the Hg odd-MIF signatures of Hg^0 evasion from the forest floor to represent the signal of Hg re-emission induced by photoreduction and microbial reduction in soil. Our earlier work has verified that soil pore Hg^0 was dominantly produced by microbial reduction, which would induce the extra odd-MIF transition.[17,34] Thus, the soil pore Hg^0 induced by microbial reduction should have the same odd-MIF signatures as the corresponding soil Hg. Therefore, the 0−10 cm soil Hg odd-MIF signature was applied to represent the signal of Hg^0 evasion caused by pore gas diffusion. We used the Hg odd-MIF value in near-surface air to represent the signature of direct atmospheric Hg^0 deposition.

https://doi.org/10.1021/acs.est.3c01222
Environ. Sci. Technol. 2023, 57, 10686−10695

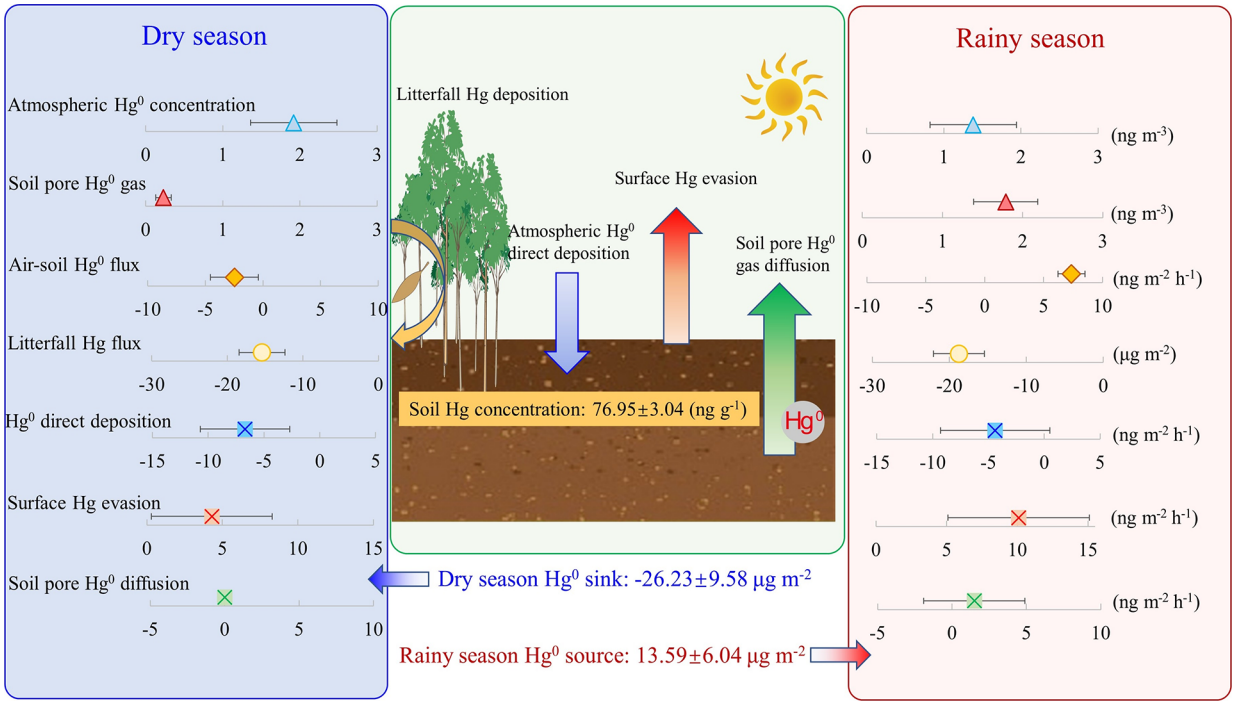

Figure 4. Difference in Hg concentration and flux (mean ± SD) between dry and rainy seasons at the P55 tropical rainforest site. Soil Hg concentration and litterfall Hg flux are from Xia et al.[17] The positive flux means Hg emission from the forest soil to the atmosphere, while the negative flux means atmospheric Hg^0 deposition into the forest soil.

The model results (Figure 4) show that the direct atmospheric Hg^0 deposition is 4.4 ± 4.9 ng m^{-2} h^{-1} in the rainy season and 6.7 ± 4.0 ng m^{-2} h^{-1} in the dry season. This can be explained by the higher atmospheric Hg^0 level in the dry season (1.80 ± 0.98 versus 1.57 ± 0.52 ng m^{-3}). The Hg evasion from the surface soil is 10.1 ± 5.0 ng m^{-2} h^{-1} in the rainy season and 4.3 ± 4.0 ng m^{-2} h^{-1} in the dry season. The soil pore Hg^0 gas diffusion flux is estimated to be 1.5 ± 3.4 ng m^{-2} h^{-1} in the rainy season and close to zero in the dry season. Since litterfall Hg deposition derived from foliage uptake of atmospheric Hg^0 represents an important atmospheric Hg input,[10,63] the overall Hg^0 mass balance over the forest floor includes direct atmospheric Hg^0 deposition, litterfall Hg deposition, Hg^0 evasion from soil, and soil pore Hg^0 gas diffusion. Combined with the litterfall deposition of 15.4 ± 3.1 μg m^{-2} in the dry season and 18.7 ± 3.3 μg m^{-2} in the rainy season,[17] the net exchange of atmospheric Hg^0 at this site is −26.2 ± 9.6 μg m^{-2} in the dry season (sink) and 13.6 ± 6.0 μg m^{-2} in the rainy season (source). It is noted that the estimation of sink and source still has uncertainties since the recent study in the alpine forest indicated that the other atmospheric Hg deposition terms possibly contain the Hg derived from the atmospheric Hg^0 sources (e.g., throughfall).[64] We recommend further studies to focus on this issue.

Up to 90% of Hg^0 re-emission dominantly driven by microbial reduction during the sampling period is by evasion over the forest floor in the tropical forest. This is different from the result in the subtropical evergreen forest at Mt. Ailao where 2/3 of Hg re-emission is from soil pore Hg^0 gas diffusion.[34] The relatively rapid litter decomposition in the tropical forest (>95% mass loss within a year[13]) causes a fast cycling of nutrients and a lower organic content in 0−10 cm soil, in contrast to the subtropical forest (e.g., 2.9% in this study versus 25.8% in the Mt. Ailao subtropical forest[21]). Meanwhile, the soil organic matter content would further control the soil−air Hg^0 flux, showing that the elevated organic matter content induced the higher Hg^0 re-emission from soil pore gas diffusion in subtropical forests.[34] In addition, tropical rainforests have a warmer and wetter climate, which promotes Hg reduction in and re-emission from soil.[65,66] The larger Hg^0 re-emission from the tropical rainforest floor results in a lower Hg concentration in surface soil. The large Hg^0 re-emission is mainly attributed to microbial Hg reduction over the forest floor. The canopy shading and low organic matter in tropical forests constrain Hg^{II} photoreduction induced by organic matter.[17] Rapid litter decomposition caused by microbial reduction promotes Hg^0 re-emission over the tropical forest floor.

We estimated a net sink of −12.6 μg m^{-2} $year^{-1}$ atmospheric Hg^0 in this tropical rainforest. The Mt. Ailao subtropical forest is a larger atmospheric Hg^0 sink with a flux of −53.9 μg m^{-2} $year^{-1}$ by micrometeorological measurements,[67] although the litterfall Hg deposition in the Mt. Ailao subtropical forest is comparable to the deposition in this tropical rainforest (34.1 ± 4.5 μg m^{-2} $year^{-1}$ versus 31.6 ± 6.5 μg m^{-2} $year^{-1}$).[17,19] The weaker atmospheric Hg^0 sink in the tropical rainforest also explains its relatively lower soil Hg concentration compared to the values in subtropical forests (70−90 ng g^{-1} in tropical rainforests versus 200−300 ng g^{-1}).[17,20,21]

At this study site and the Mt. Ailao subtropical forest site,[34] a significant anti-correlation between direct Hg^0 deposition and atmospheric Hg^0 concentration was evident [F_{Hg} = (− 4.53 ± 0.97) Hg^0_{air} + (2.18 ± 1.59), R^2 = 0.58], as shown in Figure 5. This regression relationship quantifies the dominant effect of atmospheric Hg^0 concentration on limiting direct Hg^0 deposition at both forest sites. The direct Hg^0 deposition flux to the forest floor is nearly 1.5 times the litterfall Hg flux (48.6 ± 13.0 versus 34.1 ± 6.5 μg m^{-2} $year^{-1}$) at this tropical site.[17] The Hg^0 exchange flux on the ecosystem scale using the

https://doi.org/10.1021/acs.est.3c01222
Environ. Sci. Technol. 2023, 57, 10686−10695

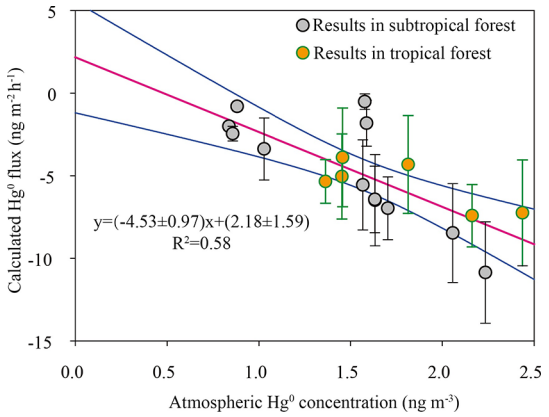

Figure 5. Flux of direct atmospheric Hg^0 deposition versus the near-surface atmospheric Hg^0 concentration. The pink line represents the regression line, and the blue lines show the 95% confidence interval. The subtropical forest results are from Yuan et al.[34]

microclimatological measurements is 2−3 times higher than the litterfall deposition flux, implying that the other deposition pathways are not considered fully.[67,68] Therefore, litterfall Hg deposition is insufficient to represent the total Hg^0 deposition to the forest floor.

4.3. Model Uncertainties. Uncertainties of the model results arise from the assumption of Hg isotopic signatures of endmembers. The isotopic signal of Hg^0 efflux under Hg-free gas exposure in the dry season was applied as the signature of an evasion endmember without considering the potential seasonal variation, thus contributing to uncertainties. In addition, the Hg isotopic composition of soil pore Hg^0 gas was not measured due to the limited sample size of soil pore gas, although this should not significantly influence the modeling results. This is because microbial reduction does not induce the odd-MIF shift,[35,36] and although the abiotic dark reduction can lead to a small MIF shift, the reduction rate is limited in the soil profiles.[37] Our earlier study has shown that soil pore Hg^0 inherits the odd-MIF value of surface soil.[34] Furthermore, given the isotopic mixing of photoreduction and microbial reduction in surface soil, it is not possible to separate the flux contribution caused by an individual reduction process. Given the extensive canopy shielding of sunlight, photoreduction should be comparatively weaker compared to microbial reduction. Finally, the measurements presented in this work cannot represent the heterogeneities of the forest floor and thus may cause model uncertainties. It is noted that the flux measurements were conducted in two months representing the dry and rainy reasons, and the data were utilized for annual flux estimates. The dynamic flux chamber measurements and the modified meteorological condition in the chamber[45] could induce additional uncertainties in this assessment.

5. ENVIRONMENTAL IMPLICATIONS

Using the Hg isotopic mass balance model, we estimated the direct atmospheric Hg^0 deposition at this site to be -4.4 ± 4.9 ng m^{-2} h^{-1}, surface soil Hg^0 evasion to be 10.1 ± 5.0 ng m^{-2} h^{-1}, and soil pore Hg^0 gas diffusion to be 1.5 ± 3.4 ng m^{-2} h^{-1} in the rainy season and -6.7 ± 4.0, 4.3 ± 4.0 ng m^{-2} h^{-1}, and near-to-zero in the dry season. Combined with the litterfall Hg flux,[17] the tropical forest floor acts as a source in the rainy season with a net flux of 13.6 ± 6.0 μg m^{-2}, while as a sink in the dry season with a net flux of -26.2 ± 9.6 μg m^{-2}. In addition, direct atmospheric Hg^0 deposition most likely exceeds litterfall Hg deposition. Using the regression equation and the mean atmospheric Hg^0 concentration in global forests (1.2−1.6 ng m^{-3}),[48] direct atmospheric Hg^0 deposition in forests is approximately 1448 ± 184 Mg $year^{-1}$ (detailed results in SI Table S4), comparable to the global litterfall deposition (1180−1500 Mg $year^{-1}$).[4,10] Furthermore, up to 90% of legacy Hg re-emission is from the tropical forest floor, and fast Hg cycling in the surface soil leads to Hg depletion in surface soil even with the Hg loading from litterfall. This study demonstrates that stable Hg isotope techniques are capable of quantifying the contribution of individual Hg biogeochemical processes during air−soil Hg^0 exchange in forest ecosystems. In the studied Chinese tropical rainforest, legacy Hg re-emission from the forest floor greatly reduces the atmospheric Hg^0 sink in tropical forests. We recommend further studies to construct the mass balance of Hg in tropical forests to verify this hypothesis.

■ ASSOCIATED CONTENT

Supporting Information

The Supporting Information is available free of charge at https://pubs.acs.org/doi/10.1021/acs.est.3c01222.

Additional experimental datasets, field observations and sample collections, summary of air−soil Hg^0 concentration and flux measured by the flux chamber technique and environmental factors, Hg isotopic composition of Hg^0 samples during rainy and dry seasons, calculation of direct Hg^0 deposition, atmospheric Hg^0 concentration, scatterplot of isotopic signatures vs Hg^0 exchange flux, vertical distribution of soil pore Hg^0 gas concentrations, and interplays of environmental factors and Hg^0 concentration (PDF)

■ AUTHOR INFORMATION

Corresponding Authors

Xun Wang − *State Key Laboratory of Environmental Geochemistry, Institute of Geochemistry, Chinese Academy of Sciences, Guiyang 550081, China;* orcid.org/0000-0002-7407-8965; Email: wangxun@mail.gyig.ac.cn

Xinbin Feng − *State Key Laboratory of Environmental Geochemistry, Institute of Geochemistry, Chinese Academy of Sciences, Guiyang 550081, China;* orcid.org/0000-0002-7462-8998; Email: fengxinbin@vip.skleg.cn

Authors

Wei Yuan − *State Key Laboratory of Environmental Geochemistry, Institute of Geochemistry, Chinese Academy of Sciences, Guiyang 550081, China;* orcid.org/0000-0003-3329-2081

Che-Jen Lin − *Center for Advances in Water and Air Quality, Lamar University, Beaumont, Texas 77710, United States*

Qinghai Song − *CAS Key Laboratory of Tropical Forest Ecology, Xishuangbanna Tropical Botanical Garden, Chinese Academy of Sciences, Mengla 666303, China*

Hui Zhang − *State Key Laboratory of Environmental Geochemistry, Institute of Geochemistry, Chinese Academy of Sciences, Guiyang 550081, China*

Fei Wu − *State Key Laboratory of Environmental Geochemistry, Institute of Geochemistry, Chinese Academy of*

https://doi.org/10.1021/acs.est.3c01222
Environ. Sci. Technol. 2023, 57, 10686−10695

Sciences, Guiyang 550081, China; University of Chinese Academy of Sciences, Beijing 100049, China

Nantao Liu − *State Key Laboratory of Environmental Geochemistry, Institute of Geochemistry, Chinese Academy of Sciences, Guiyang 550081, China; College of Resources and Environment, Southwest University, Chongqing 400715, China*

Huazheng Lu − *CAS Key Laboratory of Tropical Forest Ecology, Xishuangbanna Tropical Botanical Garden, Chinese Academy of Sciences, Mengla 666303, China*

Complete contact information is available at: https://pubs.acs.org/10.1021/acs.est.3c01222

Notes

The authors declare no competing financial interest.

■ ACKNOWLEDGMENTS

This work was funded by the National Natural Science Foundation of China (42007307 and 41921004), Youth Innovation Promotion Association CAS (grant 2022404 and 2023418), and Guizhou Provincial 2020 Science and Technology Subsidies (No. GZ2020SIG). We appreciate the Xishuangbanna Station for Tropical Rain Forest Ecosystem Studies (XSTRE) for providing plot images, climate information, and assistance in the field study. We also thank Dr. Luxiang Lin, Dr. Yun Deng, and Mr. Hong Ma for sampling in the field. The data used in this study are tabulated in SI.

■ REFERENCES

(1) Schroeder, W. H.; Munthe, J. Atmospheric mercury - An overview. *Atmos. Environ.* **1998**, *32*, 809−822.

(2) Agnan, Y.; Le Dantec, T.; Moore, C. W.; Edwards, G. C.; Obrist, D. New Constraints on Terrestrial Surface Atmosphere Fluxes of Gaseous Elemental Mercury Using a Global Database. *Environ. Sci. Technol.* **2016**, *50*, 507−524.

(3) Wang, X.; Yuan, W.; Lin, C. J.; Feng, X. B. Mercury cycling and isotopic fractionation in global forests. *Crit. Rev. Environ. Sci. Technol.* **2022**, *52*, 3763−3786.

(4) Zhou, J.; Obrist, D. Global Mercury Assimilation by Vegetation. *Environ. Sci. Technol.* **2021**, *55*, 14245−14257.

(5) Jiskra, M.; Wiederhold, J. G.; Skyllberg, U.; Kronberg, R. M.; Hajdas, I.; Kretzschmar, R. Mercury deposition and re-emission pathways in boreal forest soils investigated with Hg isotope signatures. *Environ. Sci. Technol.* **2015**, *49*, 7188−7196.

(6) Demers, J. D.; Blum, J. D.; Zak, D. R. Mercury isotopes in a forested ecosystem: Implications for air-surface exchange dynamics and the global mercury cycle. *Global Biogeochem. Cycles* **2013**, *27*, 222−238.

(7) Lindberg, S. E.; Price, J. L. Airborne Emissions of Mercury from Municipal Landfill Operations: A Short-Term Measurement Study in Florida. *J. Air Waste Manage. Assoc.* **1999**, *49*, 520−532.

(8) Lindberg, S. E.; Hanson, P. J.; Meyers, T. P.; Kim, K. H. Air/surface exchange of mercury vapor over forests - The need for a reassessment of continental biogenic emissions. *Atmos. Environ.* **1998**, *32*, 895−908.

(9) FAO. *The State of the World's Forests 2020*; 2021.

(10) Wang, X.; Bao, Z.; Lin, C. J.; Yuan, W.; Feng, X. Assessment of Global Mercury Deposition through Litterfall. *Environ. Sci. Technol.* **2016**, *50*, 8548−8557.

(11) Wang, X.; Yuan, W.; Lin, C. J.; Zhang, L.; Zhang, H.; Feng, X. Climate and Vegetation As Primary Drivers for Global Mercury Storage in Surface Soil. *Environ. Sci. Technol.* **2019**, *53*, 10665−10675.

(12) Potapov, P.; Li, X.; Hernandez-Serna, A.; Tyukavina, A.; Hansen, M. C.; Kommareddy, A.; Pickens, A.; Turubanova, S.; Tang, H.; Silva, C. E.; Armston, J.; Dubayah, R.; Blair, J. B.; Hofton, M. Mapping global forest canopy height through integration of GEDI and Landsat data. *Rem. Sens. Environ.* **2021**, *253*, No. 112165.

(13) Powers, J. S.; Montgomery, R. A.; Adair, E. C.; Brearley, F. Q.; DeWalt, S. J.; Castanho, C. T.; Chave, J.; Deinert, E.; Ganzhorn, J. U.; Gilbert, M. E.; González-Iturbe, J. A.; Bunyavejchewin, S.; Grau, H. R.; Harms, K. E.; Hiremath, A.; Iriarte-Vivar, S.; Manzane, E.; De Oliveira, A. A.; Poorter, L.; Ramanamanjato, J.-B.; Salk, C.; Varela, A.; Weiblen, G. D.; Lerdau, M. T. Decomposition in tropical forests: a pan-tropical study of the effects of litter type, litter placement and mesofaunal exclusion across a precipitation gradient. *J. Ecol.* **2009**, *97*, 801−811.

(14) Sayer, E. J.; Banin, L. F. Tree Nutrient Status and Nutrient Cycling in Tropical Forest—Lessons from Fertilization Experiments. In *Tropical Tree Physiology: Adaptations and Responses in a Changing Environment*; Goldstein, G.; Santiago, L. S., Eds.; Springer International Publishing: Cham, 2016; pp 275−297.

(15) Strassburg, B. B. N.; Kelly, A.; Balmford, A.; Davies, R. G.; Gibbs, H. K.; Lovett, A.; Miles, L.; Orme, C. D. L.; Price, J.; Turner, R. K.; Rodrigues, A. S. L. Global congruence of carbon storage and biodiversity in terrestrial ecosystems. *Conserv. Lett.* **2010**, *3*, 98−105.

(16) Cavanaugh, K. C.; Gosnell, J. S.; Davis, S. L.; Ahumada, J.; Boundja, P.; Clark, D. B.; Mugerwa, B.; Jansen, P. A.; O'Brien, T. G.; Rovero, F.; Sheil, D.; Vasquez, R.; Andelman, S. Carbon storage in tropical forests correlates with taxonomic diversity and functional dominance on a global scale. *Glob. Ecol. Biogeograph.* **2014**, *23*, 563−573.

(17) Xia, S.; Yuan, W.; Lin, L.; Yang, X.; Feng, X.; Li, X.; Liu, X.; Chen, P.; Zeng, S.; Wang, D.; Su, Q.; Wang, X. Latitudinal gradient for mercury accumulation and isotopic evidence for post-depositional processes among three tropical forests in Southwest China. *J. Hazard. Mater.* **2022**, *429*, No. 128295.

(18) Yuan, W.; Wang, X.; Lin, C. J.; Zhang, H.; Feng, X. B.; Lu, Z. Y. Impacts of Extreme Weather on Mercury Uptake and Storage in Subtropical Forest Ecosystems. *J. Geophys. Res.: Biogeosci.* **2022**, *127*, No. e2021JG006681.

(19) Wang, X.; Yuan, W.; Lu, Z. Y.; Lin, C. J.; Yin, R. S.; Li, F.; Feng, X. B. Effects of Precipitation on Mercury Accumulation on Subtropical Montane Forest Floor: Implications on Climate Forcing. *J. Geophys. Res.: Biogeosci.* **2019**, *124*, 959−972.

(20) Lu, Z.; Yuan, W.; Luo, K.; Wang, X. Litterfall mercury reduction on a subtropical evergreen broadleaf forest floor revealed by multi-element isotopes. *Environ. Pollut.* **2021**, *268*, No. 115867.

(21) Yuan, W.; Wang, X.; Lin, C. J.; Wu, C.; Zhang, L.; Wang, B.; Sommar, J.; Lu, Z.; Feng, X. Stable Mercury Isotope Transition during Postdepositional Decomposition of Biomass in a Forest Ecosystem over Five Centuries. *Environ. Sci. Technol.* **2020**, *54*, 8739−8749.

(22) Juillerat, J. I.; Ross, D. S.; Bank, M. S. Mercury in litterfall and upper soil horizons in forested ecosystems in Vermont, USA. *Environ. Toxicol. Chem.* **2012**, *31*, 1720−1729.

(23) Gómez-Armesto, A.; Méndez-López, M.; Pérez-Rodríguez, P.; Fernández-Calviño, D.; Arias-Estévez, M.; Nóvoa-Muñoz, J. C. Litterfall Hg deposition to an oak forest soil from southwestern Europe. *J. Environ. Manage.* **2020**, *269*, No. 110858.

(24) Wright, G.; Gustin, M. S.; Weiss-Penzias, P.; Miller, M. B. Investigation of mercury deposition and potential sources at six sites from the Pacific Coast to the Great Basin, USA. *Sci. Total Environ.* **2014**, *470*−*471*, 1099−1113.

(25) Wright, L. P.; Zhang, L. M.; Marsik, F. J. Overview of mercury dry deposition, litterfall, and throughfall studies. *Atmos. Chem. Phys.* **2016**, *16*, 13399−13416.

(26) Magarelli, G.; Fostier, A. H. Influence of deforestation on the mercury air/soil exchange in the Negro River Basin, Amazon. *Atmos. Environ.* **2005**, *39*, 7518−7528.

(27) Carpi, A.; Fostier, A. H.; Orta, O. R.; dos Santos, J. C.; Gittings, M. Gaseous mercury emissions from soil following forest loss and land use changes: Field experiments in the United States and Brazil. *Atmos. Environ.* **2014**, *96*, 423−429.

(28) Almeida, M. D.; Marins, R. V.; Paraquetti, H. H.; Bastos, W. R.; Lacerda, L. D. Mercury degassing from forested and open field soils in Rondonia, Western Amazon, Brazil. *Chemosphere* **2009**, *77*, 60−66.
(29) Bash, J. O.; Miller, D. R.; Meyer, T. H.; Bresnahan, P. A. Northeast United States and Southeast Canada natural mercury emissions estimated with a surface emission model. *Atmos. Environ.* **2004**, *38*, 5683−5692.
(30) Zhang, H.; Lindberg, S. E.; Marsik, F. J.; Keeler, G. J. Mercury air/surface exchange kinetics of background soils of the Tahquamenon River watershed in the Michigan Upper Peninsula. *Water, Air, Soil Pollut.* **2001**, *126*, 151−169.
(31) Wang, X.; Lin, C. J.; Feng, X. Sensitivity analysis of an updated bidirectional air-surface exchange model for elemental mercury vapor. *Atmos. Chem. Phys.* **2014**, *14*, 6273−6287.
(32) Zhu, W.; Sommar, J.; Lin, C. J.; Feng, X. Mercury vapor air-surface exchange measured by collocated micrometeorological and enclosure methods - Part I: Data comparability and method characteristics. *Atmos. Chem. Phys.* **2015**, *15*, 685−702.
(33) Guedron, S.; Amouroux, D.; Tessier, E.; Grimaldi, C.; Barre, J.; Berail, S.; Perrot, V.; Grimaldi, M. Mercury Isotopic Fractionation during Pedogenesis in a Tropical Forest Soil Catena (French Guiana): Deciphering the Impact of Historical Gold Mining. *Environ. Sci. Technol.* **2018**, *52*, 11573−11582.
(34) Yuan, W.; Wang, X.; Lin, C. J.; Sommar, J. O.; Wang, B.; Lu, Z.; Feng, X. Quantification of Atmospheric Mercury Deposition to and Legacy Re-emission from a Subtropical Forest Floor by Mercury Isotopes. *Environ. Sci. Technol.* **2021**, *55*, 12352−12361.
(35) Kritee, K.; Blum, J. D.; Johnson, M. W.; Bergquist, B. A.; Barkay, T. Mercury stable isotope fractionation during reduction of Hg(II) to Hg(0) by mercury resistant microorganisms. *Environ. Sci. Technol.* **2007**, *41*, 1889−1895.
(36) Kritee, K.; Blum, J. D.; Barkay, T. Mercury stable isotope fractionation during reduction of Hg(II) by different microbial pathways. *Environ. Sci. Technol.* **2008**, *42*, 9171−9177.
(37) Zheng, W.; Hintelmann, H. Nuclear field shift effect in isotope fractionation of mercury during abiotic reduction in the absence of light. *J. Phys. Chem. A* **2010**, *114*, 4238−4245.
(38) Zheng, W.; Hintelmann, H. Isotope fractionation of mercury during its photochemical reduction by low-molecular-weight organic compounds. *J. Phys. Chem. A* **2010**, *114*, 4246−4253.
(39) Zhao, H.; Meng, B.; Sun, G.; Lin, C. J.; Feng, X.; Sommar, J. Chemistry and Isotope Fractionation of Divalent Mercury during Aqueous Reduction Mediated by Selected Oxygenated Organic Ligands. *Environ. Sci. Technol.* **2021**, *55*, 13376−13386.
(40) Motta, L. C.; Kritee, K.; Blum, J. D.; Tsz-Ki Tsui, M.; Reinfelder, J. R. Mercury Isotope Fractionation during the Photochemical Reduction of Hg(II) Coordinated with Organic Ligands. *J. Phys. Chem. A* **2020**, *124*, 2842−2853.
(41) Fei, X.; Song, Q.; Zhang, Y.; Liu, Y.; Sha, L.; Yu, G.; Zhang, L.; Duan, C.; Deng, Y.; Wu, C.; Lu, Z.; Luo, K.; Chen, A.; Xu, K.; Liu, W.; Huang, H.; Jin, Y.; Zhou, R.; Li, J.; Lin, Y.; Zhou, L.; Fu, Y.; Bai, X.; Tang, X.; Gao, J.; Zhou, W.; Grace, J. Carbon exchanges and their responses to temperature and precipitation in forest ecosystems in Yunnan, Southwest China. *Sci. Total Environ.* **2018**, *616−617*, 824−840.
(42) Cao, M.; Zou, X.; Warren, M.; Zhu, H. Tropical Forests of Xishuangbanna, China. *Biotropica* **2006**, *38*, 306−309.
(43) Zhu, H.; Cao, M.; Hu, H. Geological History, Flora, and Vegetation of Xishuangbanna, Southern Yunnan, China. *Biotropica* **2006**, *38*, 310−317.
(44) Yuan, W.; Wang, X.; Lin, C. J.; Sommar, J.; Lu, Z. Y.; Feng, X. B. Process factors driving dynamic exchange of elemental mercury vapor over soil in broadleaf forest ecosystems. *Atmos. Environ.* **2019**, *219*, No. 117047.
(45) Lin, C. J.; Zhu, W.; Li, X.; Feng, X.; Sommar, J.; Shang, L. Novel dynamic flux chamber for measuring air-surface exchange of Hg(o) from soils. *Environ. Sci. Technol.* **2012**, *46*, 8910−8920.
(46) Fu, X. W.; Heimburger, L. E.; Sonke, J. E. Collection of atmospheric gaseous mercury for stable isotope analysis using iodine- and chlorine-impregnated activated carbon traps. *J. Anal. Atom Spectrom.* **2014**, *29*, 841−852.
(47) Zhang, H.; Fu, X. W.; Lin, C. J.; Shang, L. H.; Zhang, Y. P.; Feng, X. B.; Lin, C. Monsoon-facilitated characteristics and transport of atmospheric mercury at a high-altitude background site in southwestern China. *Atmos. Chem. Phys.* **2016**, *16*, 13131−13148.
(48) Sprovieri, F.; Pirrone, N.; Bencardino, M.; D'Amore, F.; Carbone, F.; Cinnirella, S.; Mannarino, V.; Landis, M.; Ebinghaus, R.; Weigelt, A.; Brunke, E. G.; Labuschagne, C.; Martin, L.; Munthe, J.; Wangberg, I.; Artaxo, P.; Morais, F.; Barbosa, H. D. J.; Brito, J.; Cairns, W.; Barbante, C.; Dieguez, M. D.; Garcia, P. E.; Dommergue, A.; Angot, H.; Magand, O.; Skov, H.; Horvat, M.; Kotnik, J.; Read, K. A.; Neves, L. M.; Gawlik, B. M.; Sena, F.; Mashyanov, N.; Obolkin, V.; Wip, D.; Bin Feng, X.; Zhang, H.; Fu, X. W.; Ramachandran, R.; Cossa, D.; Knoery, J.; Marusczak, N.; Nerentorp, M.; Norstrom, C. Atmospheric mercury concentrations observed at ground-based monitoring sites globally distributed in the framework of the GMOS network. *Atmos. Chem. Phys.* **2016**, *16*, 11915−11935.
(49) Fu, X.; Zhang, H.; Liu, C.; Zhang, H.; Lin, C. J.; Feng, X. Significant Seasonal Variations in Isotopic Composition of Atmospheric Total Gaseous Mercury at Forest Sites in China Caused by Vegetation and Mercury Sources. *Environ. Sci. Technol.* **2019**, *53*, 13748−13756.
(50) Wang, X.; Luo, J.; Yuan, W.; Lin, C. J.; Wang, F.; Liu, C.; Wang, G.; Feng, X. Global warming accelerates uptake of atmospheric mercury in regions experiencing glacier retreat. *Proc. Natl. Acad. Sci. U. S. A.* **2020**, *117*, 2049−2055.
(51) Sun, R. Y.; Enrico, M.; Heimburger, L. E.; Scott, C.; Sonke, J. E. A double-stage tube furnace-acid-trapping protocol for the preconcentration of mercury from solid samples for isotopic analysis. *Anal. Bioanal. Chem.* **2013**, *405*, 6771−6781.
(52) *US EPA Method 1631: Revision E: Mercury in water by oxidation, purge and trap, and cold vapor atomic fluorescence spectrometry*; 2002.
(53) Bergquist, B. A.; Blum, J. D. Mass-dependent and -independent fractionation of hg isotopes by photoreduction in aquatic systems. *Science* **2007**, *318*, 417−420.
(54) Estrade, N.; Carignan, J.; Sonke, J. E.; Donard, O. F. X. Measuring Hg Isotopes in Bio-Geo-Environmental Reference Materials. *Geostand. Geoanal. Res.* **2010**, *34*, 79−93.
(55) Yu, B.; Fu, X.; Yin, R.; Zhang, H.; Wang, X.; Lin, C. J.; Wu, C.; Zhang, Y.; He, N.; Fu, P.; Wang, Z.; Shang, L.; Sommar, J.; Sonke, J. E.; Maurice, L.; Guinot, B.; Feng, X. Isotopic Composition of Atmospheric Mercury in China: New Evidence for Sources and Transformation Processes in Air and in Vegetation. *Environ. Sci. Technol.* **2016**, *50*, 9262−9269.
(56) Giovanella, P.; Cabral, L.; Bento, F. M.; Gianello, C.; Camargo, F. A. Mercury (II) removal by resistant bacterial isolates and mercuric (II) reductase activity in a new strain of Pseudomonas sp. B50A. *New Biotechnol.* **2016**, *33*, 216−223.
(57) Obrist, D.; Pokharel, A. K.; Moore, C. Vertical profile measurements of soil air suggest immobilization of gaseous elemental mercury in mineral soil. *Environ. Sci. Technol.* **2014**, *48*, 2242−2252.
(58) Zhou, J.; Wang, Z.; Zhang, X.; Driscoll, C. T. Measurement of the Vertical Distribution of Gaseous Elemental Mercury Concentration in Soil Pore Air of Subtropical and Temperate Forests. *Environ. Sci. Technol.* **2021**, *55*, 2132−2142.
(59) Moore, C. W.; Castro, M. S. Investigation of factors affecting gaseous mercury concentrations in soils. *Sci. Total Environ.* **2012**, *419*, 136−143.
(60) Sigler, J. M.; Lee, X. Gaseous mercury in background forest soil in the northeastern United States. *J. Geophys. Res.: Biogeosci.* **2006**, *111*, G02007.
(61) Ericksen, J. A.; Gustin, M. S.; Xin, M.; Weisberg, P. J.; Fernandez, G. C. Air-soil exchange of mercury from background soils in the United States. *Sci. Total Environ.* **2006**, *366*, 851−863.
(62) Gustin, M. S.; Engle, M.; Ericksen, J.; Lyman, S.; Stamenkovic, J.; Xin, M. Mercury exchange between the atmosphere and low mercury containing substrates. *Appl. Geochem.* **2006**, *21*, 1913−1923.

https://doi.org/10.1021/acs.est.3c01222
Environ. Sci. Technol. 2023, 57, 10686−10695

(63) Yuan, W.; Sommar, J.; Lin, C. J.; Wang, X.; Li, K.; Liu, Y.; Zhang, H.; Lu, Z.; Wu, C.; Feng, X. Stable Isotope Evidence Shows Re-emission of Elemental Mercury Vapor Occurring after Reductive Loss from Foliage. *Environ. Sci. Technol.* **2019**, *53*, 651−660.
(64) Wang, X.; Yuan, W.; Lin, C. J.; Luo, J.; Wang, F.; Feng, X.; Fu, X.; Liu, C. Underestimated Sink of Atmospheric Mercury in a Deglaciated Forest Chronosequence. *Environ. Sci. Technol.* **2020**, *54*, 8083−8093.
(65) Lin, C. J.; Gustin, M. S.; Singhasuk, P.; Eckley, C.; Miller, M. Empirical models for estimating mercury flux from soils. *Environ. Sci. Technol.* **2010**, *44*, 8522−8528.
(66) Johnson, D. W.; Benesch, J. A.; Gustin, M. S.; Schorran, D. S.; Lindberg, S. E.; Coleman, J. S. Experimental evidence against diffusion control of Hg evasion from soils. *Sci. Total Environ.* **2003**, *304*, 175−184.
(67) Wang, B.; Yuan, W.; Wang, X.; Li, K.; Lin, C. J.; Li, P.; Lu, Z.; Feng, X.; Sommar, J. Canopy-Level Flux and Vertical Gradients of Hg(0) Stable Isotopes in Remote Evergreen Broadleaf Forest Show Year-Around Net Hg(0) Deposition. *Environ. Sci. Technol.* **2022**, *56*, 5950−5959.
(68) Obrist, D.; Roy, E. M.; Harrison, J. L.; Kwong, C. F.; Munger, J. W.; Moosmuller, H.; Romero, C. D.; Sun, S.; Zhou, J.; Commane, R. Previously unaccounted atmospheric mercury deposition in a midlatitude deciduous forest. *Proc. Natl. Acad. Sci. U. S. A.* **2021**, *118*, No. e2105477118.

https://doi.org/10.1021/acs.est.3c01222
Environ. Sci. Technol. 2023, 57, 10686−10695